Pulsed-laser assisted nanopatterning of metallic layers combined with atomic force microscopy

S. M. Huang,[a] M. H. Hong, Y. F. Lu, B. S. Lukỳanchuk, W. D. Song, and T. C. Chong
Data Storage Institute and Department of Electrical & Computer Engineering, Laser Microprocessing Laboratory, National University of Singapore, 10 Kent Ridge Crescent, Singapore 117608

(Received 2 October 2001; accepted for publication 11 December 2001)

Pulsed-laser assisted nanopatterning of metallic layers on silicon substrates under an atomic force microscope (AFM) tip has been investigated. A 532 nm Nd:YAG pulsed laser with a pulse duration of 7 ns was used. Boron doped silicon tips were used in contact mode. This technique enables processing of structures with a lateral resolution down to 10 nm on the copper layers. Nanopatterns such as pit array and multilines with lateral dimensions between 10 and 60 nm and depths between 1.5 and 7.0 nm have been created. The experimental results and mechanism of the nanostructure formation are discussed. The created features were characterized by AFM, scanning electron microscope and Auger electron spectroscopy. The apparent depth of the created pit has been studied as a function of laser intensity or laser pulse numbers. Dependence of nanoprocessing on the geometry parameters of the tip and on the optical and thermal properties of the processed sample has also been investigated. Thermal expansion of the tip, the field enhancement factor underneath the tip, and the sample surface heating were estimated. It is proposed that field-enhancement mechanism is the dominant reason for this nanoprocessing. © *2002 American Institute of Physics.*
[DOI: 10.1063/1.1448882]

I. INTRODUCTION

Continuing miniaturization of electronic and mechanic devices has led in recent years to an intense interest in the generation of nanometer-sized structures on the surfaces. As the traditional masking approach in optical lithography is limited to a minimal resolvable feature size of half a wavelength of the light, $\lambda/2$, many alternative techniques have been developed. One approach in this respect consisted of the illumination of the tip of a scanning tunneling microscope (STM) with a pulsed laser. Structures with lateral dimensions below 30 nm and therefore well below $\lambda/2$ could be produced underneath the tip.[1–4] This method has limited applications since it can only be used for special materials and certain ambient conditions (e.g., vacuum). The other approach is an atomic force microscope (AFM) combined with a pulsed laser. This method, with much wider applications compared to the first technique, was first suggested by Wessel,[5] and was discussed in more detail by Stockmann.[6] Recently, this method has been used to create hillocks and pits with dimensions down to 20 nm on materials including gold, gold/palladium, polymethyl methacrylate (PMMA), and polycarbonate.[7,8]

Despite the prominent interest in the photoassisted STM or AFM techniques, the main reason for the structuring process remains unclear and is controversially discussed by many groups. On one hand field, enhancement in the vicinity of the tip and subsequent field evaporation is proposed, while the thermal effects are ruled out.[1–4,7–9] On the other hand, mechanical contact as a result of thermal expansion is discussed as well.[10–13]

In this study, the nanostructure fabrication on metallic surfaces using a pulsed laser in combination with an AFM is reported. Nanopatterns such as pit and multilines were created. Dependence of pit apparent depth on the laser fluence and laser pulse numbers has been investigated. Chemical components of the modified features were analyzed by Auger electron spectroscopy (AES). The morphologies of created features were characterized by AFM and scanning electron microscope (SEM). Thermal expansion of the tip, the field enhancement underneath the tip and the sample heating were estimated. Experimental results and mechanisms of nanostructure formation are discussed. We hope that our experiments will contribute further to the study of mechanisms of the photoassisted nanoprocessing.

II. EXPERIMENTAL DETAILS

The experiments were carried out on a commercial scanning probe microscopy (SPM) system (Autoprobe CP, Park Scientific Instruments). The SPM probe head has an open architecture, which allows an external laser beam irradiation directly on the tip and sample. The sample is made of a copper or aluminum film with a thickness of 35 nm on Si substrate. The metallic films were deposited by sputtering method. During imaging and nanoprocessing, the tip was fixed and the sample was moved via a tube scanner. A 532 mn Nd:YAG pulsed laser with a pulse duration of 7 ns was used. The maximum repetition rate of the laser is 10 Hz. The laser beam is vertically polarized. The laser beam was focused by a plano-convex lens (focal length $f=20$ cm). The laser spot diameter, D_b, was estimated using the second har-

[a]Author to whom correspondence should be addressed; electronic mail: smhuang@dsi.nus.edu.sg

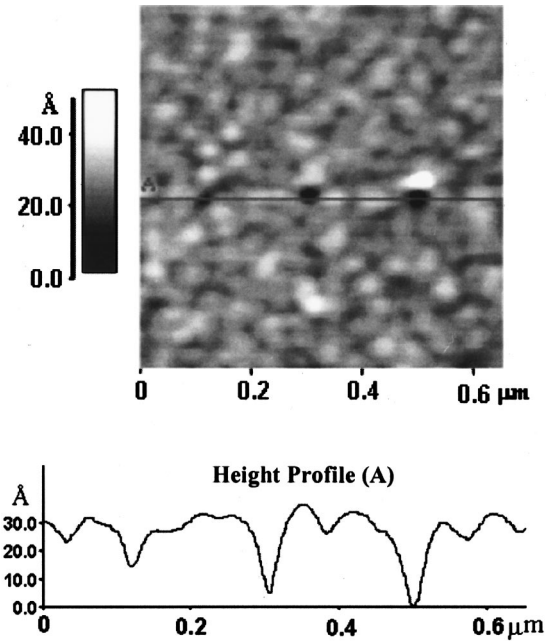

FIG. 1. AFM image and the height profile of the nanohole created by one pulse with laser intensities of 7.5, 8, and 8.5 MW/cm^2, respectively.

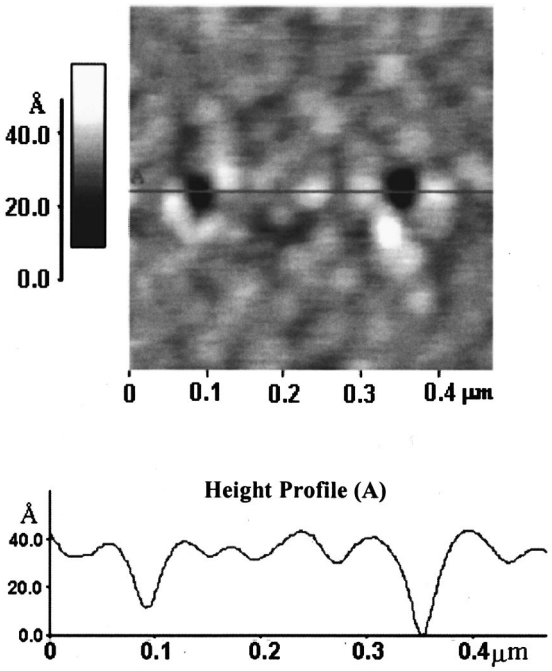

FIG. 2. AFM image and the height profile of the nanohole created by one pulse with laser intensities of 11 and 12 MW/cm^2, respectively.

monic divergence ($\alpha \cong 1.5 \times 10^{-3}$ rad) as $D_b \cong \alpha f \cong 300\ \mu$m. The laser beam was focused on the tip apex. The laser alignment was performed under an optical charge coupled device microscope with high resolution. It was adjusted by observing the diffraction ring from the tip. The laser beam hits the sample surface at an incidence angle of $\theta_i \sim 80°$, measured from the surface normal. The SPM was operated in AFM mode. Boron doped silicon (0.001 Ω cm) tip (Park Scientific Instruments) was used in contact mode.

III. RESULTS

The laser beam is introduced to the gap between the tip and the copper sample. When the laser intensity is above a threshold value, one pulse can create one pit on the copper surface. We estimated a threshold level of ~7.5 MW/cm^2 for the Si tips (Park Scientific Instruments, Ultralevels™, cantilevel type A and B) in contact mode. A Si tip B was used to obtain pits. Figure 1 shows three pits created by laser pulses. Each pit was induced by a single shot. The nanoholes, from the left to the right, were created with pulse intensities of 7.5, 8, and 8.5 MW/cm^2, respectively. The height profile of the nanoholes is also shown in Fig. 1. The depths of the three nanoholes are 1.54, 2.43, and 3.20 nm, and their full widths are 31.4, 39.2, and 43.1 nm, respectively. With higher pulse intensity, the created nanohole becomes even deeper and wider. Figure 2 presents the two pits created by two pulses with the laser intensities of 11 and 12 MW/cm^2, respectively. The height profile of both pits is also shown in Fig. 2. Their depths are 5.47 and 7.05 nm, and their widths are 58.6 and 62.2 nm, respectively.

Dependence of the pit depth on the laser intensity is presented in Fig. 3. The depths were measured from the pits created by single laser pulse with different laser intensities, for example, the pits shown in Figs. (1) and (2). From Fig. 3, the pit depth displays a linear increase with the laser intensity. In addition, the pit depth can increase with more laser shots. The relationship between the depth of the pit and the pulse number is presented in Fig. 4. The depths were measured from the pit created by different pulse number but with the same laser intensity. The depth tends to saturate after several laser shots.

In order to obtain continuous lines using a pulsed laser, the scanning speed must be slow enough. Figures 5(a) and (b) show AFM image and the height profile of a series of created lines on the copper surface, respectively. The laser beam with an intensity of 8 MW/cm^2 and repetition rate of 10 Hz was used. The scanning speed was 0.02 μm/s. An Ultralevels™ Si tip A was used. The line width is about 10

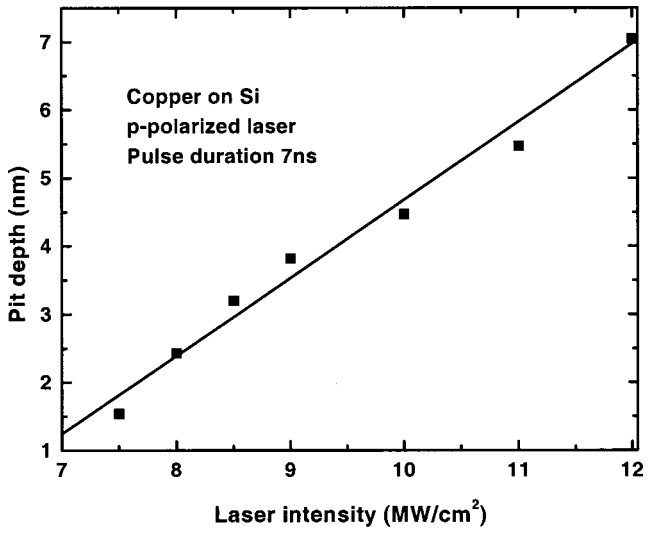

FIG. 3. Dependence of nanohole apparent depth on the laser intensity.

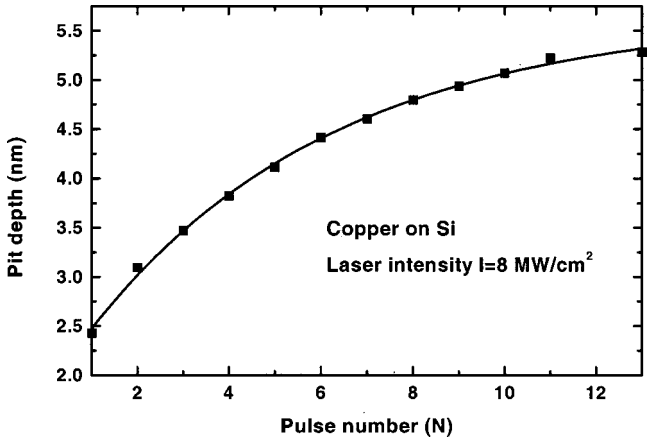

FIG. 4. Dependence of nanohole apparent depth on the laser pulse number.

nm and the depth is about 2.7 nm as shown in Fig. 5(b). With higher laser intensity, the continuous line created becomes wider and deeper. Figures 6(a) and (b) present AFM image and the height profile of the lines created with a laser intensity of 10 MW/cm^2, respectively. The line width is about 18 nm and the depth is about 5.0 nm shown in Fig. 6(b). After laser nanoprocessing, SEM analyses of the AFM tips were done. No damages were found on the shapes of tips, even after thousands of laser shots, if the laser intensity used is in the parameter condition shown in Fig. 1. Chemical components of created nanostructures were analyzed by AES. AES line scan and point survey analyses were done. No Si signal was observed in all these AES analyses. Figure 7 shows Auger spectra from four points at centers or edges of a created nanostructure by laser.

IV. DISCUSSION

In this section we discuss several possible mechanisms of nanoprocessing with the pulsed laser irradiation of the AFM tip–sample gap. To understand the basic mechanism, it is necessary to calculate the temperatures of the tip and the sample. Because the size of the tip apex is smaller than the wavelength of the laser, macroscopic or geometrical optics is not applicable to the case any more. The electric fields on the tip, on the sample, and in the free space should be calculated by an exact solution of the Maxwell equations. The temperature distribution can be calculated by solving three dimensional heat flow equations. The laser energy absorbed by the tip should be calculated using the theory of the light scattering and with knowledge of the exact geometry of the tip–surface junction.[14,15] The thermal deformation of the tip should also be considered. Moreover, the situation may be complicated by the surface polariton generation and various waveguide effects.[16] To the best of our knowledge this complex problem has not been solved. In this work, we restrict ourselves by using simplified approaches that we believe still give correct order of magnitude estimation.

A. Tip heating by pulsed laser

When a laser beam is introduced to the gap between the tip and the sample, the absorption of the laser energy leads to an increase of the tip temperature. In this work, the laser

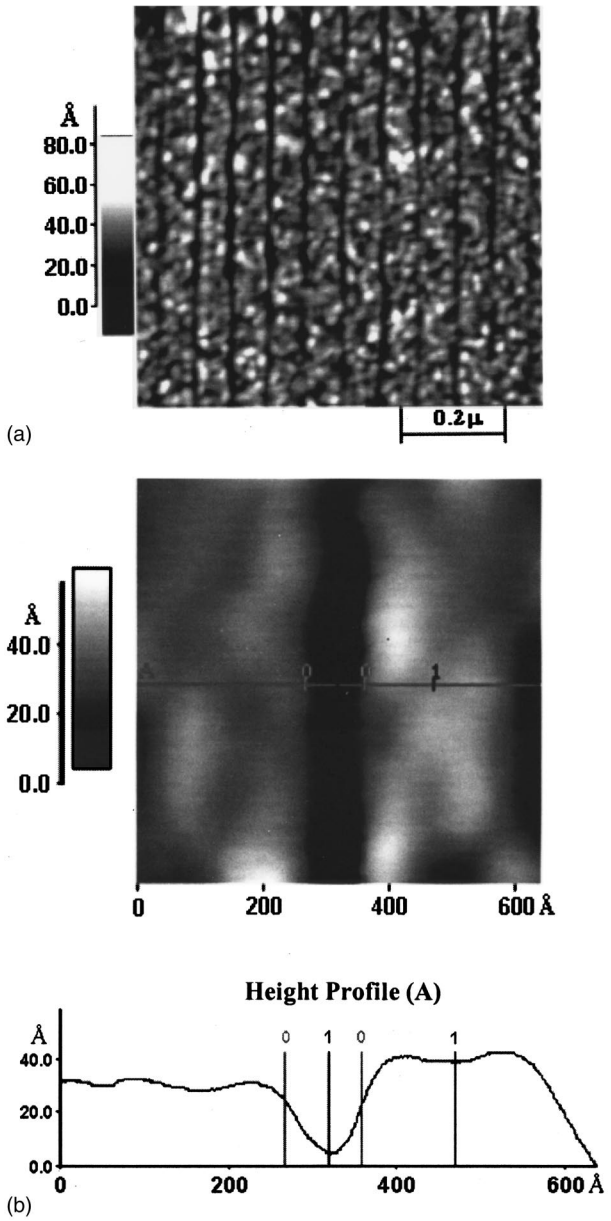

FIG. 5. AFM image and the height profile of multinanolines created with a laser intensity of 8 MW/cm^2: (a) AFM image, (b) height profile.

incidence angle is $\theta_i \sim 80°$, measured from the surface normal. Three characteristic dimensions should be considered:[17] (i) the photon absorption length, $\lambda_{abs}=9400$ Å, for Si; (ii) the thermal diffusion length, $\lambda_{th} \sim (\chi\tau)^{1/2} \cong 7937$ Å, here $\chi=0.9$ cm^2 s^{-1},[18] the Si coefficient of thermal diffusion; (iii) the laser beam size, $D_b \cong 300\,\mu$m. Since $D_b \gg \lambda_{abs} > \lambda_{th}$, steady state heating cannot be established during the pulse duration and the maximum transient temperature occurs at the end of the laser pulse and is approximately proportional to the laser fluence.[17] SEM images of Si tips A and B before laser irradiation are shown in Figs. 8(a) and (b), respectively. After laser irradiation and AFM images of created nanostructures being obtained, the shape of the tip showed no distortion except that occasionally a few fine and loose clusters were found attached to the top of tip. These clusters on the tip can be cleaned using laser. The apex tip radius from Fig. 8, $r_t \sim (330-820)$ Å, is much smaller than λ_{th}, therefore, the

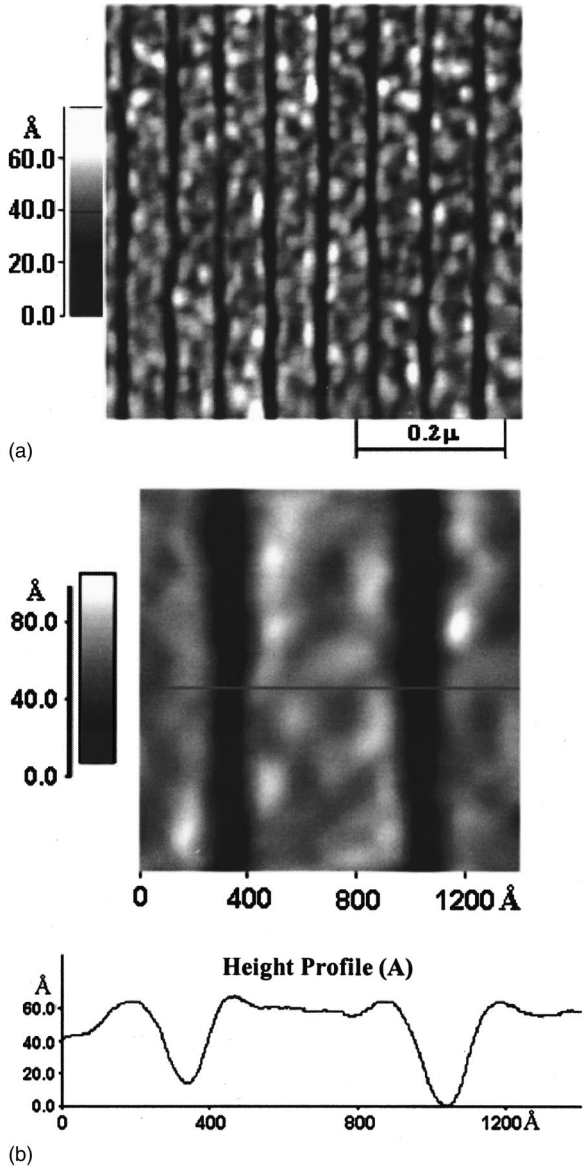

FIG. 6. AFM image and the height profile of multinanolines created with a laser intensity of 10 MW/cm^2: (a) AFM image, (b) height profile.

case is not strictly one dimensional. A three-dimensional case with an azimuthal symmetry was considered by Miskovky *et al.*[19] It was found that the temperature rise in the conical tip due to surface generation of heat varies almost linearly with laser intensity and heating time and depends strongly on the cone angle and thermal properties.

For an estimation of the transient temperature in the λ_{th} vicinity of the tip apex, one may use a simple expression introduced by Ukraintsev *et al.*:[10]

$$\Delta T_{tip} \cong \frac{6\theta_0 E_p(1-\bar{R})}{\pi^2(1-\cos\theta_0)\lambda_{th} D_b^2 c_p \rho}, \tag{1}$$

where c_p and ρ are the heat capacity and the density of the silicon, respectively, θ_0 is the tip cone angle in radians, E_p is the laser pulse energy, and $\bar{R}$ is the effective reflectivity of the light averaged over the irradiated tip surface and hence over the different incidence angles.

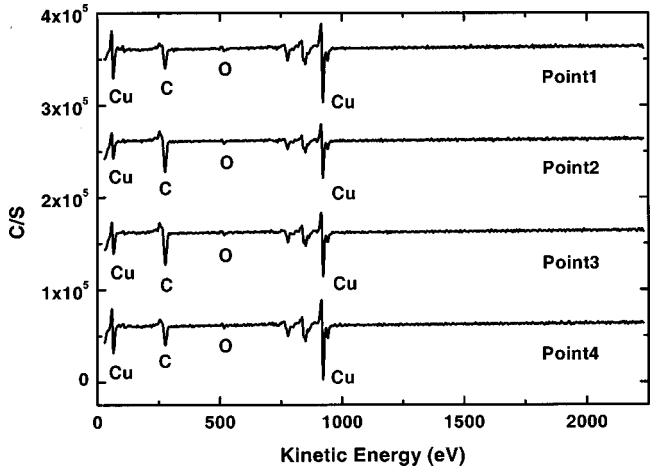

FIG. 7. AES from four points at centers or edges of a nanostructure created by laser.

According to Ukraintsev's work, the coarse estimation from Eq. (1) is in good agreement with the comprehensive 3D calculation done by Miskovsky *et al.*[19] Then for silicon, $\bar{R}=0.5$, $\lambda_{th}=7.9\times10^{-5}$ cm, $D_b=0.03$ cm, $c_p=0.71$ Jg^{-1} K^{-1}, and $\rho=2.33$ g cm^{-3}. The tip cone angle θ_0 can be estimated from SEM images of Si tip A and B shown in Figs.

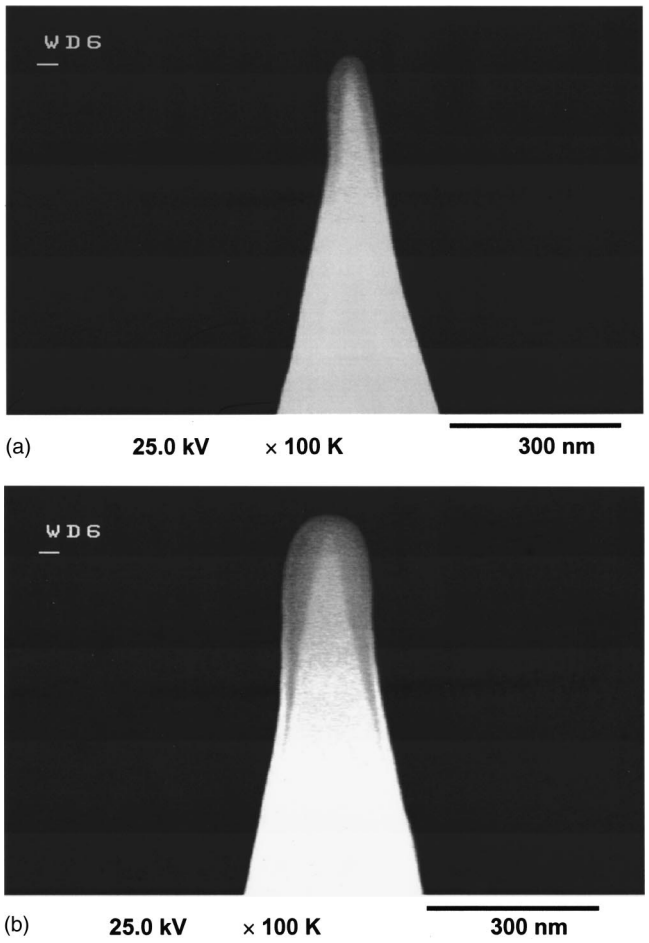

FIG. 8. SEM images of two types of Si tips before laser irradiation: (a) tip A. (b) Tip B.

8(a) and (b). For tip B, $\theta_0 = 0.49$ rad (or 28°), and for tip A, $\theta_0 = 0.35$ rad (or 20°). From Eq. (1), one can obtain

$$\Delta T_{\text{tipB}} \cong (1.0\times 10^7\ E_p)\ \text{K or } 10\ \text{K at } E_p = 1\ \mu\text{J for tip B}, \tag{2}$$

and

$$\Delta T_{\text{tipA}} \cong (1.4\times 10^7\ E_p)\ \text{K or } 14\ \text{K at } E_p = 1\ \mu\text{J for tip A}. \tag{3}$$

For the conditions of this experiment, a laser pulse power intensity 1 MW/cm^2=4.9 μJ/pulse. From Eqs. (2) and (3), the temperature rise of the tips is about 350–800 °C within our process window.

B. Tip thermal expansion

An expansion of the tip induced by laser at the vicinity of the thermal diffusion length λ_{th}, and at the tip apex will have the strongest impact on the tip–sample gap induction. An expansion within the surface layer of the tip with a thickness of λ_{th} and separated from the apex by several λ_{th} lengths will not affect the gap reduction, since its major expansion direction is virtually normal to the tip axis. Therefore, the tip thermal expansion may be estimated as:[10]

$$\Delta S_{\text{tip}} \cong \alpha\eta\lambda_{\text{th}}\Delta T_{\text{tip}}, \tag{4}$$

where η is the tip geometry factor in the range from 1 to 3 depending on the tip cone angle, α is the coefficient of the linear thermal expansion, and ΔT_{tip} is the temperature rise of the tip induced by laser irradiation. For silicon, $\alpha = 3.8\times 10^{-6}$ K^{-1}.[18] Assuming $\eta=2$ and employing Eqs. (2) and (3), one has $\Delta S_{\text{tipB}} \cong (6.0\times 10^5 E_p)$ Å for tip B, and $\Delta S_{\text{tipA}} \cong (8.4\times 10^5 E_p)$ Å for tip A. The thermal expansion of the Si tips is about 2–5 nm in our process window. The thermal expansion of the tip is of the same order of magnitude as the depth of nanopits and nanolines presented in the Sec. III. Despite this, it will be shown that the thermal expansion of the tip may not be a main reason for nanoprocessing in the following section.

C. Sample surface heating and field enhancement

Energy balance methods and a semi-infinite mode are conventionally used to estimate the temperature rise of the sample. With a metallic semi-infinite mode, heat produced in the sample spread quickly over a large volume, and the temperature rise of the sample is only a few degrees. If it is considered that the sample is made of a thin metal sheet with a high thermal conductivity placed on a dielectric with a small thermal conductivity, one can expect a different result. The heat encounters a much larger thermal resistance while spreading over the thin sheet, which leads to a higher temperature in the sample surface.

Let us consider a Cu sheet having a thickness of 35 nm. The sheet is placed on the semi-infinite Si support. The thermal conductivity of Si is smaller than that of copper. A laser beam is irradiated on the sample surface with an incidence angle θ_i. Simulation of laser interactions with materials (SLIM©)[20] of one layer and multilayer structures can be employed to calculate the thermal effects of this problem.

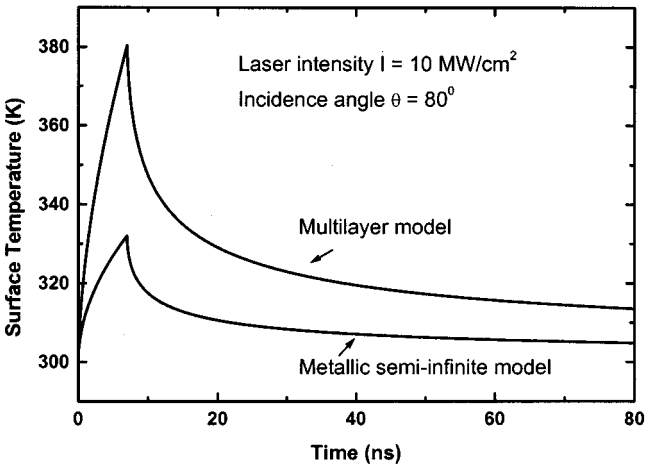

FIG. 9. Computed surface temperature for the Cu semi-infinite model and multilayer model with a laser intensity of 10 MW/cm^2 and an incidence angle of 80°.

Figure 9 shows the computed surface temperature for the Cu semi-infinite model and multilayer model with a laser intensity of 10 MW/cm^2 and an incidence angle of 80°. The maximal temperature rise of the sample surface is 32 and 80 K for these two models, respectively. Figure 10 presents the computed surface temperature with a laser intensity of 10 MW/cm^2 and an incidence angle of 0°. The maximal temperature of the sample surface is 492 and 931 K for these two models, respectively. The temperature rise using the multilayer model is two times larger than using the metallic semi-infinite model. In our work, we did find that nanopatterning was hard to be realized in bulk metallic materials. From the multilayer model and for the normal incidence, if the intensity increases to 1.5 times 10 MW/cm^2, the temperature can reach up to the melting point of Cu, if the intensity increases to 8 times 10 MW/cm^2, the temperature can rise up to the evaporation point of Cu.

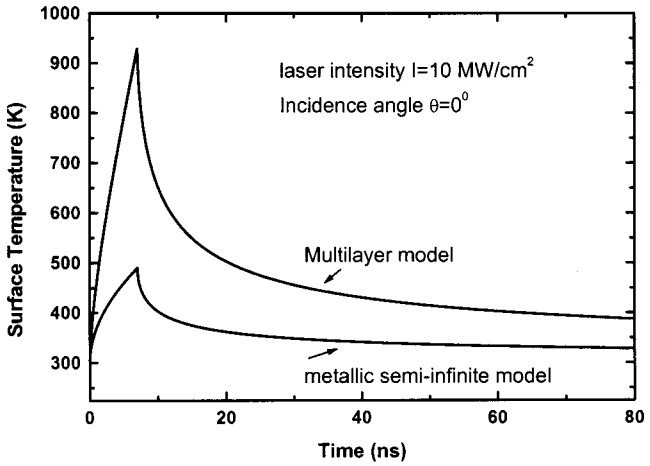

FIG. 10. Computed surface temperature for the Cu semi-infinite model and multilayer model with a laser intensity of 10 MW/cm^2 and an incidence angle of 0°.

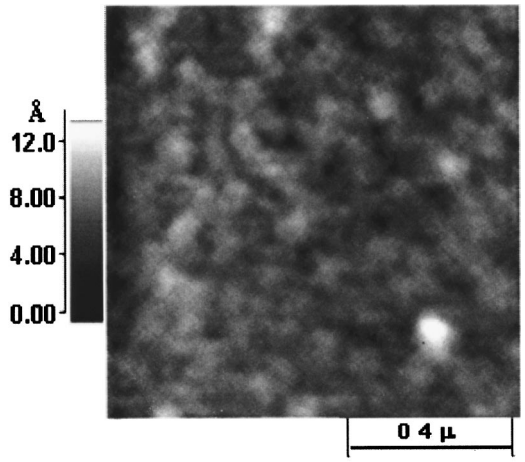

FIG. 11. AFM image of a Cu film surface without laser treatment.

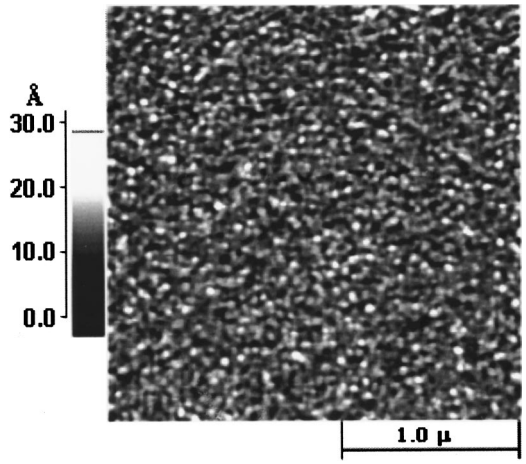

FIG. 12. AFM image of a Cu film surface after several laser shots with a intensity of 10 MW/cm^2.

Now, let us go back to our experiment. When a laser beam is introduced to the gap between the tip and the sample with an incidence angle of $\theta_i = 80°$. An enhanced optical field forms underneath the tip. The enhanced optical field can be expected to locally heat the sample surface in a very small domain. The field enhancement factor near the irradiated AFM tip in nanoprocessing can be estimated by the well-known model of a small dielectric spheroid.[21,22] The field enhancement factor β has a simple expression:

$$\beta = \left| \frac{\epsilon}{1+(\epsilon-1)A} \right|, \tag{5}$$

where ϵ is the complex dielectric constant and A is the depolarization factor, which depends on the axis ratio $r = a/b$ of the spheroid,

$$A(r) = \frac{1}{2r^2} \int_0^\infty \frac{1}{(s+1)^{3/2}(s+r^{-2})}\, ds. \tag{6}$$

The dielectric constant of Si is 17.14 ± 0.37 i. For the Si tips A and B, the axis ratio r is about 2.73 and 1.9, respectively. From Eqs. (5) and (6), Si tips A and B have optical enhancement β^2 of 32 and 16.

The diffracted and scattered light beams from the tip have different incidence angles for the sample surface. Our problem is much more complicated than that of SLIM© model. However, SLIM model can be used to estimate the thermal effects in our system. If we consider the optical enhancement $\beta^2 = 16$ (for tip B) and average effect of different incidence angles together, assuming these two factors happen to be canceled, a temperature distribution similar to Fig. 10 can be obtained for our situation and for an intensity of 10 MW/cm^2. The maximal temperature rise is about several hundred degrees.

In this work, we emphasize the phenomena observed in the interaction of the surface with laser irradiation. Figure 11 shows an AFM image of a Cu film without laser treatment. The surface is very smooth with an average roughness of 1.02 Å. The highest data point minus the lowest is 1.31 nm within the area shown in Fig. 11. At this surface condition, we found that no nanopit could be obtained by one laser shot, even with an intensity high enough to cause damage to the tip. Although this single pulse laser irradiation could reduce the thermal expansion of the tip with the same order of magnitude as the depth of the nanopit and nanoline described in Sec. III, no nanomodification was achieved at this condition. Therefore, the mechanical contact forces between the tip and the sample induced by the thermal expansion of the tip is not strong enough to do nanoprocessing of the surface.

In order to realize nanopatterning of the sample surface, a few laser pulses are needed to modify the surface. Figure 12 shows an AFM image of the sample surface after several shots with an intensity of about 10 MW/cm^2. Laser irradiation of the sample induced its surface reorganization. Isolated crystals of 30–50 nm in size can be seen on the top surface. The surface is with an average roughness of 2.03 Å, and the maximum peak-to valley distance is 2.83 nm, within the area shown in Fig. 12. The surface becomes relatively a little rough, compared with the film without laser treatment shown in Fig. 11. At the surface condition shown in Fig. 12, nanopit and nanolines can be obtained, as shown in Figs. 1, 2, 5, and 6. At this condition, the reflectivity of the sample surface can be expected to decrease, compared with the surface shown in Fig. 11. On the other hand, the heat encounters even higher thermal resistance while spreading over the surface than we mentioned in the system consisting of a thin and smooth metallic sheet attached to a massive dielectric support with a smaller thermal conductivity. Therefore, even higher temperature rise in the sample surface can be obtained. The thermal effects over this kind of surface system were studied by Geshev *et al.*[23,24] They reported the temperature distribution calculations on the laser-illuminated scanning probe tips using both an effective finite-difference algorithm and Fourier–Bessel transformation methods. Their studies show that for the film layer with small thin confined objects having nanometer size the temperature can reach several thousands of degrees while the tip is still far away from this temperature. Thus, the material can be successfully nanoprocessed. Their theoretical study results greatly coincide with our results. Based on Geshev *et al.*'s results and the configurations of the nanopits and nanolines presented in Sec. III, we could attribute the formation of these nanostruc-

tures to occurrence of rapid melting or evaporation in nano-sized domains of the sample during the nanoprocessing.

From the above discussion, there are various factors that may play roles in the photoassisted nanoprocessing. We think that the field enhancement mechanism is the main reason for this nanoprocessing. The enhanced field of the tip locally heats the sample to the melting and evaporation temperature in a nano-sized domain of the sample. We think the thermal expansion of the tip also make some contribution to the fabrication of the nanopatterns. The thermal expansion of the tip decreases the gap between the tip and the sample and increases the light intensity at the nanoprocessing point further, resulting in higher temperature in a nano-sized domain on the sample. On the other hand, the thermal expansion of the tip decreases the distance between the tip and grains, leading to an increasing repulsive force between them. It seems that this phenomenon includes another physical mechanism, mechanical contact mechanism.[2,10–13] In our work, we did not find distortion of the tip after thousands of laser pulses with the intensity up to 12 MW/cm^2. During the processing, if the tip did contact the sample surface due to the thermal expansion of the tip, and a strong repulsive force did appear between the tip and grains on the sample, the tip should be worn down quickly. Moreover, even if the film surface was at the condition shown in Fig. 12, no matter how the setting point for the AFM tip was increased and the distance between the tip and the sample was decreased, no nanopit or nanoline could be created without laser assistance. Finally, we find that it is very hard to pattern a sample whose surface layer has high transmittance or low absorptance for the used green laser. For example, a sample consisted of an Al thin film on the Si substrate. The Al thin film has low absorptance for the laser used. It is found that Al surface is hard to be modified unless the laser intensity is extremely high, resulting in the damage of the Si tip. Thus, we think that mechanical contact force due to the thermal expansion of the tip may not be a main reason for the nanoprocessing within our process window. If the laser intensity is very high and out of our process window, the mechanical contact force due to the thermal expansion of the tip might be a main reason for the patterning processing. From the nanoprocessing results using different shape of Si tips described in Sec. III and the processing results on different surfaces mentioned in this section, we can see that the nanoprocessing depends strongly on the material properties of not only the tip but also the sample surface. The geometry parameters of the tip, the curvature radius of the tip and the solid angle of the probe cone, also have great influence on the final results.

V. CONCLUSION

Nanopatterning of metallic layers on silicon substrates were carried out by laser irradiation under an AFM tip. Processing of structures with a lateral resolution down to 10 nm are realized on copper layers using this technique. Nanopit array and multiple-nanoline patterns have been created. The created features were characterized by AFM, SEM, and Auger electron spectroscopy. The apparent depth of the created nanoholes can be controlled by laser intensity or laser numbers. The nanoprocessing strongly depends on the geometry parameters of the Si tip, the optical and thermal properties of the sample, including the properties of the metallic layer and the substrate. The thermal expansion of the tip, field enhancement underneath the tip, and the sample surface heating during the laser irradiation all have contribution to the fabrication of the nanostructures, however the tip enhanced laser irradiation mechanism might be the main reason.

[1] A. A. Gorbunov and W. Pompe, Phys. Status Solidi A **145**, 333 (1994).
[2] J. Jersch and K. Dickmann, Appl. Phys. Lett. **68**, 868 (1996).
[3] Y. F. Lu, Z. H. Mai, G. Qiu, and W. K. Chim, Appl. Phys. Lett. **75**, 2359 (1999).
[4] Y. F. Lu, Z. H. Mai, Y. W. Zheng, and W. D. Song, Appl. Phys. Lett. **76**, 1200 (2000).
[5] J. Wessel, J. Opt. Soc. Am. **B2**, 1538 (1985).
[6] M. Stockmann, Avtometriya **3**, 30 (1989) [in Russian].
[7] J. Jersch, F. Demming, and K. Dickmann, Appl. Phys. A: Mater. Sci. Process. **64**, 29 (1997).
[8] J. Jersch, F. Demming, L. J. Hildenhagen, and K. Dickmann, Appl. Phys. A: Mater. Sci. Process. **66**, 29 (1998).
[9] H. J. Mamin, P. H. Guethner, and D. Rugar, Phys. Rev. Lett. **65**, 2418 (1990).
[10] V. A. Ukraintsev and J. T. Yates, Jr., J. Appl. Phys. **80**, 2561 (1996).
[11] I. Lyubinetsky, Z. Dohnálek, V. A. Ukraintsev, and J. T. Yates, Jr., J. Appl. Phys. **82**, 4115 (1997).
[12] J. Boneberg, M. Tresp, M. Ochmann, H.-J. Münzer, and P. Leiderer, Appl. Phys. A: Mater. Sci. Process. **66**, 615 (1998).
[13] R. Huber, M. Koch, and J. Feldmann, Appl. Phys. Lett. **73**, 2521 (1998).
[14] C. F. Bohren and D. R. Huffman, *Absorption and Scattering of Light by Small Particles* (Wiley, New York, 1998).
[15] H. C. Van de Hulst, *Light Scattering by Small Particles* (Dover, New York, 1981).
[16] *Surface Polaritons*, edited by V. M. Agranovich and D. L. Mills (Elsevier, Amsterdam, 1982).
[17] J. F. Reay, *Effects of High-Power Laser Radiation* (Academic, New York, 1971), Chap 3.
[18] CRC handbook of Chemistry and Physics, 69th ed., edited by R. C. Weast (CRC, Boca Raton, FL, 1989).
[19] N. M. Miskovsky, S. H. Park, J. He, and P. H. Cutler, J. Vac. Sci. Technol. B **11**, 366 (1993).
[20] SLIM is a copyrighted program developed by Rajiv K. Singh and J. Viatella at Materials Science and Engineering Department at the University of Florida.
[21] A. Wokaun, Mol. Phys. **56**, 1 (1985).
[22] J. I. Gersten and A. Nitzan, J. Chem. Phys. **73**, 3023 (1980).
[23] P. I. Geshev, F. Demming, J. Jersch, and K. Dickmann, Thin Solid Films **368**, 156 (2000).
[24] P. I. Geshev, F. Demming, J. Jersch, and K. Dickmann, Appl. Phys. B: Lasers Opt. **70**, 91 (2000).